10 February 1997

PHYSICS LETTERS A

ELSEVIER

Physics Letters A 226 (1997) 69–74

Optical magnetic resonance imaging of Rb vapor in low magnetic fields

J. Skalla [a], G. Wäckerle [a], M. Mehring [a], A. Pines [b]

[a] *2. Physikalisches Institut, Universität Stuttgart, D-70550 Stuttgart, Germany*

[b] *Department of Chemistry, University of California, Berkeley, CA 94720-1460, USA*

Received 24 October 1996; accepted for publication 4 December 1996

Communicated by B. Fricke

Abstract

By applying magnetic field gradients to alkali vapor cells, images of the spatial distribution of spin-polarized Rb atoms were obtained. Optical pumping is used to produce precessing spin-polarization in the ground state. Detection of the coherent spin transients is performed in the time-domain by a single optical probe beam covering the whole sample cell. Spatial resolution of better than 1 mm has been achieved by a projection–reconstruction method.

PACS: 32.30.Dx; 32.80.Bx; 87.59.Pw

Keywords: Magnetic resonance imaging; Optical pumping; Magnetic resonance spectra; Alkali atoms; Zeeman effect

1. Introduction

Since its introduction in the early 1970s [1,2] nuclear magnetic resonance imaging has developed into an indispensable tool for obtaining images of heterogeneous biological tissue in a noninvasive and apparently hazard-free manner, and is widely used in medical applications. While the nuclear spin of hydrogen has been most widely used, the area of applications has been extended to other spin species (including unpaired electron spins), thus opening the door for the investigation of different kinds of materials [3].

A persistent issue in magnetic resonance imaging (MRI) is detection sensitivity. The signal amplitude is proportional to the spin magnetization which in thermal equilibrium is determined by the Boltzmann factor $\exp(-\Delta E/k_B T)$ of spin level population, where $\Delta E = \hbar\gamma B_0$ for a spin with a gyromagnetic ratio γ in a magnetic field B_0. To obtain sufficient spin magnetization MRI is usually performed at high magnetic fields in the range of several tesla.

In the field of electron paramagnetic resonance imaging (EPRI) [4], since the gyromagnetic ratio of the electron is 658 times larger than that of the proton, the sensitivity is expected to be much larger. In practice EPR sensitivity is usually not larger than the sensitivity achieved in NMR imaging. The reasons for this are the more complex EPR lineshapes and microwave losses in the material. Nevertheless a one-dimensional resolution of about 10 μm is achievable in certain cases of pulsed EPR imaging [5]. Spatial spin resolution of better than $(100\ \mu\text{m})^3$ is commonly referred to as magnetic resonance microscopy [6].

Although MRI measurements have been performed mostly in high magnetic fields, efforts have been made to work with reduced magnetic fields. In low magnetic fields, however, additional technical efforts are needed in order to enhance spin polarization. Recently,

PII S0375-9601(96)00927-9

MRI results were reported in magnetic fields of the order of 0.1 mT [7] where the nuclear spin magnetization was increased by dynamic nuclear polarization (DNP) through the electronic spins in the sample. The transfer of polarization from laser-polarized noble gases is an additional approach to the enhancement of NMR/MRI.

In the following we report on the first imaging experiments on electronic spins in the gas phase at low pressures and in magnetic fields below 0.1 mT. Due to the low number density of spins in gas-phase samples it is ineffective to detect magnetic resonance signals by conventional magnetic resonance if the spin ensemble is in thermal equilibrium. Therefore, we use optically pumped alkali atoms in the ground state together with an optical detection scheme for the magnetic resonance signals. Since optical fields are involved, we term this approach optical magnetic resonance imaging (OMRI). The use of laser light on a resonant optical transition of the atoms to be observed enhances the sensitivity by orders of magnitude compared to conventional EPR imaging methods and the imaging of even highly diluted atoms in very low fields ($\ll 10^{-4}$ T) becomes possible. The method presented here may not be restricted to gas-phase imaging. Applications to optically accessible solid state systems seems feasible as well.

In this Letter we report first results on imaging of a spatially inhomogeneous distribution of Rb spin polarization in a vapor cell. The technique is based on standard MRI procedures by applying linear magnetic field gradients to achieve spatial resolution. However, optical polarization and detection methods are used to enhance and monitor the spin resonance signals.

2. MRI Technique

In MRI a magnetic field gradient is typically superimposed on a static magnetic field in order to encode the spatial position in the Larmor frequency of spin precession. By convention the static magnetic field, B_{z0}, is applied along the z direction and the field gradients refer to the z component of the magnetic field. Contributions from gradients in the transverse plane affect the Larmor frequency only to second order and are usually ignored. In Cartesian coordinates, the imaging gradients therefore can be represented by $(G_x, G_y, G_z) = (\partial B_z/\partial x, \partial B_z/\partial y, \partial B_z/\partial z)$, or in shorthand notation by $\boldsymbol{G} = (\boldsymbol{\nabla B})_z$. In a coordinate system rotating around the z axis with the Larmor frequency of atoms positioned at $\boldsymbol{r} = 0$, the Zeeman Hamiltonian can be expressed as

$$\hat{\mathcal{H}} = \gamma \boldsymbol{r} \cdot \boldsymbol{G} \hat{F}_z, \tag{1}$$

where $\hat{F}_z$ is the spin operator of the ground state alkali atom resulting from the sum of electron and nuclear spin operators via hyperfine interaction, and γ is the effective gyromagnetic ratio of the ground state atom in low magnetic fields.

The spin precession signal is calculated from the expectation value of the transverse spin component $\hat{F}_+$ as

$$S(t) = \int_V n(\boldsymbol{r}) \mathrm{Tr}[\sigma(t) \hat{F}_+] \, \mathrm{d}V, \tag{2}$$

where $n(\boldsymbol{r})$ is the spatially inhomogeneous spin density, σ is the density matrix of the ground state spin levels, and the integral extends over the sample volume. In what follows we assume a homogeneous intensity distribution of the optical detection beam over the entire sample, because the beam cross section was larger than the cell dimensions. If this is not the case a spatial distribution function must be included in the integral of Eq. (2).

Assuming an initial transverse magnetization $\sigma(0) \sim \hat{F}_x$, created for example by a resonant $(\pi/2)$ rf pulse for example, one can evaluate Eq. (2) and the time-domain signal in the rotating frame is given by

$$S(t) = \int_V \mathcal{R}(t) n(\boldsymbol{r}) \exp[\mathrm{i} \boldsymbol{r} \cdot \boldsymbol{k}(t)] \, \mathrm{d}V \tag{3}$$

with

$$\boldsymbol{k}(t) = \gamma \int_0^t \boldsymbol{G}(t') \, \mathrm{d}t', \tag{4}$$

where a time dependence of the gradient and a spin-relaxation function $\mathcal{R}(t)$ are considered (see below). From this equation the spin density distribution $n(\boldsymbol{r})$ may be calculated by an inverse transformation, provided the exact $\boldsymbol{k}$-space trajectory is known. In most applications of two-dimensional imaging the $\boldsymbol{k}$-space is traced by means of successive gradient pulses G_y

and G_z, a technique called Fourier phase-encoding [8]. In cases where the spin relaxation is strong ($T_2 \ll 1$ ms) as in many EPR situations, constant gradients, e.g. in the y and z directions, are applied simultaneously. This so-called frequency encoding may be utilized for a projection–reconstruction type of imaging and provides a slightly better signal-to-noise ratio since it puts more weight onto k values near the origin [9].

In the two-dimensional (y, z) imaging performed here, the spin density is reproduced by an inverse Fourier transformation, which in the case of frequency-encoding is performed in polar coordinates,

$$n(y,z) = \int_0^{\pi} \int_{-\infty}^{\infty} S(k,\varphi) \exp(-\mathrm{i}\boldsymbol{k}\cdot\boldsymbol{r})|\boldsymbol{k}|\,\mathrm{d}\boldsymbol{k}\,\mathrm{d}\varphi, \tag{5}$$

where $S(k,\varphi)$ are the time-domain signals for different orientations φ of the resulting gradient $(G_y, G_z) = (G\cos\varphi, G\sin\varphi)$.

Since the alkali atoms are embedded in a buffer gas the spin signal will decay due to atomic diffusion in the applied field gradient. In the presence of a stationary gradient G the spin-precession signal will decrease with [10]

$$\begin{aligned}\mathcal{R}(t) &= \exp(-t/T_2)\exp(-\gamma^2G^2Dt^3/3)\\ &\approx \exp(-t/T_2)\exp(-t/T_2^{\star}),\end{aligned} \tag{6}$$

where D is the diffusion coefficient and T_2 is the intrinsic relaxation time due mainly to alkali spin-exchange collisions and spin-decay collisions with buffer-gas atoms or molecules. The crude approximation used in the right hand side of Eq. (6) leading to $1/T_2^{\star} = \Delta\nu = 0.6\pi(\gamma^2G^2D/3)^{1/3}$ [11] results in a diffusion limited spatial resolution Δr given by

$$\begin{aligned}\Delta r &\approx \frac{1}{\pi}\left(\frac{1}{T_2^{\star}} + \frac{1}{T_2}\right)\left(\frac{2\pi}{\gamma G}\right)\\ &= 1.2\left(\frac{D}{3\gamma G}\right)^{1/3} + \frac{2}{T_2\gamma G}.\end{aligned} \tag{7}$$

Although a stronger gradient increases the spectral linewidth, the spatial resolution is improved. However, one should bear in mind that the gradient must be small enough to avoid transverse magnetic fields comparable in magnitude to B_{z0}. In our experiments, diffusion of Rb atoms is reduced by adding 300 mbar of N_2 as a buffer gas. For a temperature of 60°C evaluation of Eq. (7) leads to $\Delta r \approx 0.3$ mm, where the following parameters, relevant in our experiments, are used, $\gamma(^{85}\mathrm{Rb}) = 2\pi \times 4.67$ MHz/mT, $G = 6$ μT/cm, $D = 1.38$ cm^2/s, and $1/T_2 \approx 10^3$ s^{-1}. Consequently sub-mm resolution of alkali atoms in the gas phase is feasible when the experimental parameters are properly adjusted.

3. Experimental results and discussion

Our sample consists of a cylindrical glass cell (length and diameter of 1 cm) and contains a droplet of natural Rb metal and 300 mbar of N_2. It is placed in the center of a cylindrical setup (length of 20 cm and diameter of 10 cm), containing a pair of Maxwell coils and two pairs of saddle coils to produce the magnetic field gradients G_y and G_z, respectively (see Fig. 1). A long solenoid (not shown in the figure) provides a homogeneous field B_{z0} parallel to the z axis. The whole setup is placed inside a one-layer μ-metal shield with 1 cm openings for the pump and detection light beams. By means of a 50% beam splitter these are aligned in parallel. To avoid any spatial distortion of the light beams by the glass cell, the light traverses its flat windows. A similar experimental setup was used in Ref. [12].

The pump beam is provided by a Ti^{3+}-sapphire laser which is circularly polarized and expanded to a beam diameter of approximately 1 cm. Optical pump pulses with a rectangular envelope are shaped by an acousto-optic modulation. The pulse duration is 5 μs and thus smaller than the Larmor period of the precessing ^{85}Rb spins in the applied magnetic field. Optical excitation is performed on the ^{85}Rb ($F = 3 \rightarrow F'$) D_1 transition, where F' denotes the excited state with unresolved hyperfine splitting. The pump pulse with an intensity of $I \approx 300$ W/m^2 creates sufficient transversal ground state magnetization which immediately starts to precess around the magnetic field of $B_{z0} = 16.69$ μT. This field is small enough to avoid any noticeable influence of the Paschen-Back effect on the magnetic resonance lineshapes, i.e. the experiments are performed in the Zeeman limit of the magnetic field strength.

To detect the optical rotation induced by the precessing anisotropic magnetization a 8 mW probe

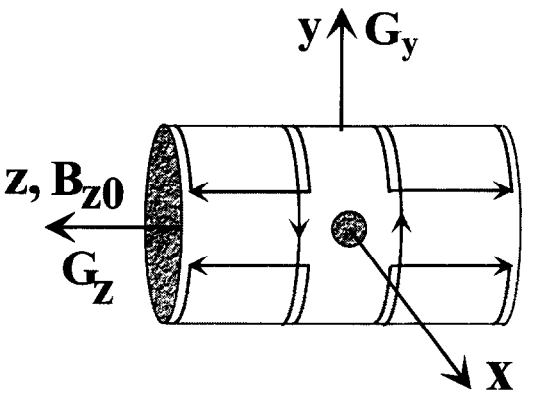

Fig. 1. Schematic of the OMRI setup. A homogeneous magnetic field B_{z0} is applied axially to the cylindrical support of the gradient coils. Two pairs of saddle coils produce a magnetic field gradient G_y, and a pair of Maxwell coils provides the gradient G_z. The laser beams for pumping and detection are adjusted in parallel and travel along the x direction. The entire setup is surrounded by a μ-metal shield (not shown in the figure). The arrows indicate the directions of currents.

beam from a current- and temperature-stabilized single-mode laser diode is expanded to a diameter of 4 cm and tuned slightly off-resonance with respect to the on-resonance pump beam. The rotation of the probe-beam polarization is detected via a polarimetric detection method [12,13]. The large probe-beam waist allows a nearly homogeneous detection sensitivity across the small glass cell. The atomic number density of the Rb atoms was controlled by maintaining the sample at a temperature of 60°C by a hot air stream. At this temperature spin-exchange collisions among the alkali atoms do not play a significant role on the time scale of the experiment.

To demonstrate the feasibility of optical magnetic resonance imaging an array of five circular apertures was placed in the pump beam just before it enters the vapor cell, thus five "tubes" of spin polarized atoms are created in the vapor cell by optical pumping. These tubes have a diameter of 1 mm and are spaced 2.2 mm apart (vertically and horizontally). The precessing spin magnetization is detected immediately after the pump pulse. Fourier transformation of the recorded time-domain signals results in the spectral densities shown in Fig. 2. They are displayed for five different orientations of the applied magnetic field gradient $|\boldsymbol{G}| = 6\ \mu$T/cm. Depending on the orientation of $\boldsymbol{G}$ one detects between two and four spectral resonances corresponding to the projections of the spatial spin density distribution on the axis perpendicular to $\boldsymbol{G}$. If no magnetic field gradient is applied, only a single line at $\nu_L = 77.95$ kHz appears. The higher amplitude of the central lines is a result of the Gaussian intensity distribution of the pump beam over the 5-pinholes mask. The linewidth of the resonances corresponds to about 1 mm spatial spread of spin-polarized alkali atoms and is not the ultimate spatial resolution possible in such a diffusion-limited experiment. Experiments with smaller pump beam diameters have shown that at least 0.5 mm can be resolved within the given glass cell. The gradient-induced change of the magnetic field across the sample region is not much smaller than B_{z0}. However, this results in a rather small error in the spatial coordinates, which is not larger than ± 0.08 mm. Other comparable or slightly larger errors result from noncompensated residual magnetic stray fields penetrating the μ-metal shield and a small remanent magnetization of the shield itself.

In order to obtain the two-dimensional spin distribution, more than five projections are necessary. We varied the orientation of the gradient $\boldsymbol{G}$ between 0° and 176° in steps of 4°. The result of a filtered back-projection of the 44 corresponding data sets according to Eq. (5) is shown in Fig. 3 where in addition to the greyscale plot two projections (in the y and z direction) are also displayed. The shape of the phantom is well reproduced. Due to a small imperfection of the array of apertures, one of the holes does not exactly fit into the square raster of the others. This imperfection is clearly resolved in the two-dimensional image.

4. Conclusion

We have demonstrated the feasibility of imaging an inhomogeneous spin distribution of gas-phase atoms in low magnetic fields. The standard scenario of magnetic resonance imaging, i.e. high magnetic fields, low temperatures, and condensed matter materials, are overcome in this case by the use of optical spin-polarization and detection techniques. As a first example we presented experimental results for low pressure Rb vapor in a buffer-gas atmosphere with approximately 3×10^{11} spin per cm^3, where two-dimensional images have been obtained with a spatial resolution of better than 1 mm. The application of the

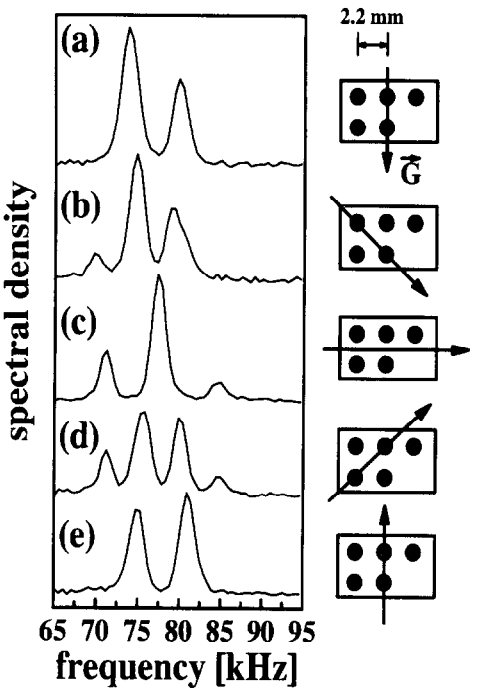

Fig. 2. Spectral density of the ^{85}Rb spin transitions for different orientations of the resulting magnetic field gradient G in the (y, z) plane. An array of five apertures (each of 1 mm diameter) was placed into the pump beam right before the sample cell. Values of the magnetic fields and gradient are $B_{z0} = 16.69$ μT and $|G| = 6$ μT/cm, respectively.

method to three dimensions is straightforward and should allow the direct detection of diffusional processes, such as edge-enhancement in surface-coated cells or the rapid decay of higher diffusional modes in cells of the present kind.

The technique might be of interest as a diagnostic tool in optimizing the production of highly polarized nuclear spin systems of noble gases, which are increasingly being used for investigations in medicine [14], basic physics research [15], and material science [16]. Polarization profiles in a high-density atomic vapor may be spatially resolved via a spin-exchange coupled second (monitor) atomic species with lower vapor pressure to avoid strong absorption of the detection beam. In this case a collision-induced polarization transfer between the different spin species is necessary [12].

OMRI need not be restricted to the gas phase. Among the large field of optical detection of magnetic resonance in the solid state a recently published experiment [17] deals with the observation of transverse alkali magnetization in solid ^{4}He. Real-time observation of the alkali spin diffusion should be observable with a resolution far beyond the $(100\ \mu\text{m})^3$ with the presented method. Other fields, where electron and nuclear spin polarization can be induced optically are quantum-well structures in GaAs [18] or other semiconductor materials, raising the possibility of applications of OMRI beyond the realm of alkali vapors.

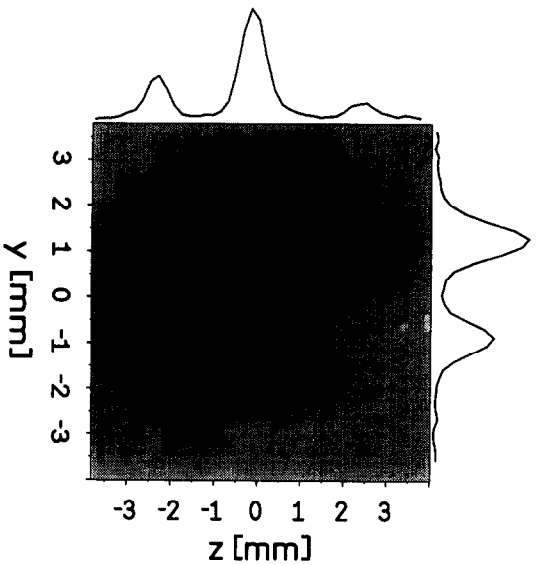

Fig. 3. Greyscale plot of the spatial spin-density distribution as obtained from filtered back projection of 44 different field-gradient orientations in the (y, z) plane. The projections onto the y axis (Fig. 2a) and the z axis (Fig. 2c) are also shown along the corresponding directions.

References

[1] P.C. Lauterbur, Nature 242 (1973) 190.
[2] P. Mansfield and P.K. Grannell, J. Phys. C 6 (1973) L422.
[3] B. Blümich and W. Kuhn, eds., Magnetic resonance microscopy: Methods and application in materials science, agriculture and biomedicine, (VCH, Weinheim, 1991).
[4] M.J.R. Hoch and A.R. Day, Solid State Commun. 30 (1979) 211.
[5] G.G. Maresch, M. Mehring and S. Emid, Physica B 138 (1986) 261;
G.G. Maresch, Ph.D. thesis, Universität Stuttgart (1987).
[6] P.T. Callaghan, Principles of nuclear magnetic resonance microscopy (Oxford Univ. Press, Oxford, 1993).

[7] G. Planinšič, T. Guiberteau and D. Grucker, J. Magn. Res. B 110 (1996) 205.
[8] A. Kumar, D. Welti and R.R. Ernst, J. Magn. Res. 18 (1975) 69.
[9] P.T. Callaghan and C.D. Eccles, J. Magn. Res. 71 (1987) 426.
[10] E.L. Hahn, Phys. Rev. 80 (1950) 580.
[11] C.B. Ahn and Z.H. Cho, Med. Phys. 16 (1989) 22.
[12] J. Skalla, G. Wäckerle and M. Mehring, Opt. Commun. 127 (1996) 31.
[13] R.V. Jones, Proc. R. Soc. A 349 (1976) 423.
[14] M.S. Albert et al., Nature 370 (1994) 199.
[15] T.E. Chupp, R.J. Hoare, R.L. Walsworth and B. Wu, Phys. Rev. Lett. 72 (1994) 2363.
[16] G. Navon et al., Science 271 (1996) 1848.
[17] S.I. Kanorsky, S. Lang, S. Lücke, S.B. Ross, T.W. Hänsch and A. Weis, Phys. Rev. A 54 (1996) R1010.
[18] J.A. Marohn et al., Phys. Rev. Lett. 75 (1995) 1364.